Effect of Powder Bed Fusion Laser Sintering on Dimensional Accuracy and Tensile Properties of Reused Polyamide 11

Urvashi Fowdar Gunputh * , Gavin Williams , Marzena Pawlik , Yiling Lu , Paul Wood

Posted Date: 18 October 2023

doi: 10.20944/preprints202310.1195.v1

Keywords: powder bed fusion laser sintering; polyamide 11; reuse; dimensional accuracy; tensile properties; crystallinity

Article

Effect of Powder Bed Fusion Laser Sintering on Dimensional Accuracy and Tensile Properties of Reused Polyamide 11

Urvashi F Gunputh *, Gavin Williams, Marzena Pawlik, Yiling Lu and Paul Wood

College of Science and Engineering, University of Derby, Quaker Way, Derby, UK; g.williams1@derby.ac.uk (G.W.); m.pawlik@derby.ac.uk (M.P.); y.lu@derby.ac.uk (Y.L.); p.wood7@derby.ac.uk (P.W.)

* Correspondence: u.gunputh@derby.ac.uk; Tel.: +44(0)1332593286

Abstract: Polyamide 11 (PA11) is a plant-based nylon made from castor beans. Powder bed fusion laser sintering (PBF-LS) is an additive manufacturing process used for PA11 which allows the reuse of the unsintered powder. The unsintered powder is mixed with virgin powders at different refresh rates which has been studied extensively for most semi-crystalline polyamides. However, there is lack of information on the effect of using 100% reused PA11 powder and the number of times it is reused on its own during powder bed fusion laser sintering. This paper investigates the effect of reusing PA11 powder in PBF-LS and number of times it is reused on the dimensional accuracy, density, thermal and tensile properties. From 100% virgin powder to 3rd use of the powder, there is a decrease in powder wastage, decrease in crystallinity and tensile strength. These was associated with the polymerisation and cross-linking process of polymer chains, upon exposure to high temperature. This results in a higher molecular weight and hence density. From the 4th use to 10th reuse, the opposite was observed which was associated to an increase in high-viscosity and unmolten particles which resulted in defects in the PBF-LS parts.

Keywords: Powder bed fusion laser sintering; polyamide 11; reuse; dimensional accuracy; tensile properties; crystallinity

1. Introduction

Powder bed fusion laser sintering, PBF-LS, is a powder-based additive manufacturing process that uses a laser beam to sinter the powder particles layer by layer. The surrounding unmolten powder supports the 3d printed part, hence there is no need for support structures. However, if the unmolten powder feedstock is not used, it would have to be disposed of, which would be wasteful, time-consuming, and expensive [1,2]. Reusing the powder from the PBF-LS process is the solution although material properties have been shown to deteriorate with this practice [3–6]. Polymers are the most commonly used material for PBF-LS [7] with polyamides being the leading thermoplastic in use [8]. Polyamide 12 (PA12) is the most widely employed polyamide due to its low cost, ease of processability, high mechanical strength [8] and higher melt temperature as compared to crystallisation temperature [9]. Nonetheless, it is petroleum-based and reuse of this powder is still associated with a certain amount of carbon dioxide emission [6]. Polyamide 11 is a plant-based nylon made from castor beans which has high strength, durability and resistance to chemicals and heat [10]. When compared to PA12, it has been shown to have a higher toughness and ductility at the expense of a slightly lower modulus and a higher hydrothermal ageing resistance [11]. With an aim of sustainable manufacturing, there is an increasing interest in the PBF-LS of PA11. The use of this powder for various applications including medical device manufacturing have been investigated [12,13] and understanding its reuse will add to standards associated with medical device manufacturing using powder based AM processes such as ASTM F3456-22.

Polyamides are semi-crystalline, that is, they have both amorphous (irregularly arranged polymer chains) and crystalline (regularly arranged polymer chains) phases. The effect of reusing polyamide powder during PBF-LS process will be dependent on how the different phases react to

 doi:10.20944/preprints202310.1195.v1

repeat high temperature exposure. Heat flow maps using a Differential Scanning Calorimetry (DSC) method has been used extensively to characterise the melting/crystallisation of PBF-LS sintered parts which reflects on the polymer chains reaction due to heating and cooling down [4,5,14]. Using such heat flow maps, virgin PA12 and polyamide 6 (PA6) sintered parts have been found to have 47% crystalline phase as compared to amorphous [15]. Reusing such polyamide powders (without mixing with fresh powder) reduced the crystallinity of the sintered parts which significantly reduced their ultimate tensile strength (UTS), elongation at break and maximum shear stress [5]. This has been associated with an increase in molecular weight with reuse which is caused by the post-condensation reaction during polymerisation of the polyamide [14]. This increase in weight reduces the mobility of the polymer chains and affects the sintering process adversely. Conversely, Yao et al. [16] associated lower density with reuse of PA2200 powder during an PBF-LS process. This reduction in density was related to the presence of voids in the sintered part which in turn caused deterioration of the mechanical properties of the latter [16]. Composites of virgin PA11, (Fresh and not mixed with reused powder), targeted for PBF-LS process exhibited 38% crystallinity [17] while virgin PA11 powder, on its own, exhibited an approximate of 30% crystallinity [18]. Virgin PA11 powder targeted for Multi Jet Fusion (MJF) process was shown to have a crystallinity of 39% while its 3d printed part had a crystallinity of 26 % [19]. The resulting MJF PA11 part had an UTS of 46 MPa and modulus of 932 MPa. However, this process is different from PBF-LS whereby there is the use of an ink agent and an infra-red lamp for the heating and fusing of powders [19]. Compression moulded sheets of PA11 have a crystal fraction of 16% [20]. MJF PA11 have higher crystallinity than compression moulded ones. There is lack of information on the effect of reusing PA11 using a PBF-LS process on the mechanical properties which creates the need to investigate reused PBF-LS PA11 parts.

Furthermore, dimensional accuracy is a major issue with powder bed fusion laser sintering [21]. It has been associated with post process cooling resulting in shrinkage/warpage [22,23] and high surface roughness, also known as the orange-peel effect, owing to unmolten powder at the edges [4,24]. This has been observed with reused PA12 [4,25] whereby ageing of the latter powders has been associated with the change in powder shape and morphology which causes powder aggregation, expansion and shrinkage. Yusoff et al. [25] further related the high viscosity of aged powder to surface roughness. There is minimal information on dimensional accuracy of reused PA11 powder during powder bed fusion laser sintering which further strengthens the need for this work.

The main objective of this work is to investigate the effect of reusing PA11 powder in a PBF-LS process on the dimensional accuracy, physical properties, crystallinity and tensile properties of the sintered part. Using a Formlabs Fuse1 printer, tensile test and density samples were first additively manufactured using 100% virgin PA11 powder. The ratio of used powder to unused powder and its associated weight were analysed. The density cubes were used for density measurements following which the tensile test pieces were tested using a Universal tester. Pieces of the sintered density cubes were analysed using Differential scanning calorimetry (DSC) to analyse crystallinity. The remaining powder in the chamber were reused up to 10 times, following which the mentioned tests were repeated. The effect of reusing the PA11 powder in PBF-LS up to 10 times was related to the crystallinity and tensile properties.

2. Materials and Methods

2.1. Powder bed fusion laser sintering of PA11

A Formlabs Fuse 1 3D printer (CREAT3D, UK) was used. It has a build volume of 16.5 × 16.5 × 30 cm, prints at a layer thickness of 110 μm with an Ytterbium fibre laser (1065 nm Wavelength; 10W) of 200 μm spot size. It works with Preform Software that is supplied with the 3D printer.

Polyamide 11 powder used in this paper was supplied by CREAT3D, UK and had the mechanical properties listed in Table 1 (Obtained from Manufacturers, Formlabs, [26]) which is the baseline for comparison in this work. The powder also had a moisture content of 0.37% and printed samples with this powder has been validated as non-cytotoxic, non-irritant and non-sensitiser in

Preprints (www.preprints.org) | NOT PEER-REVIEWED | Posted: 18 October 2023 doi:10.20944/preprints202310.1195.v1

accordance with ISO 10993-1. This means PBF-LS PA11 is safe to use as medical devices coming in contact with the skin.

Table 1. Mechanical Properties of PA 11 samples printed using the Formlabs Fuse 1 Printer and after conditioning at 50 % humidity and a temperature of 23 °C [26] .

Tensile Property	Value	Method
Ultimate Tensile Strength	49 MPa	
Tensile Modulus	1600 MPa	ASTM D 638-14
Elongation at Break (XY)	40 %	

Five tensile test pieces with dimensions as shown in Figure 1(a) were printed in the XZ direction and density cubes (Figure 1(b)) were printed top of each (Figure 1 (c)) other to increase the Z-height and therefore the amount of powder required to complete the build. A temperature of 193 °C was maintained in the build chamber during the 3D printing process.

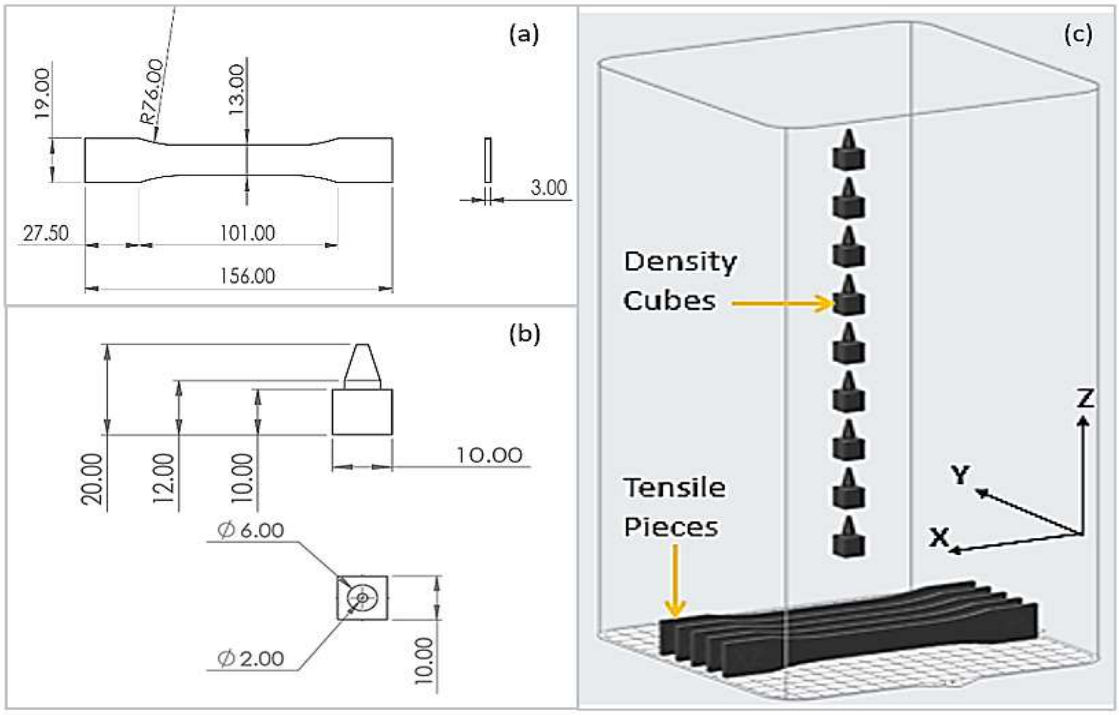

Figure 1. Shape and dimension of (**a**) Tensile Test sample and (**b**) Density Cubes; (**c**) Location of tensile test samples and density cubes in Fuse 1 Printer Build Chamber.

The same samples were manufactured 10 times. The first build used 100% virgin PA11 powder and was known as B01. Once the 3d printed parts were removed from the build, the unfused powder from the first build was sieved using a Sift 300 Sieve with Fuse Sift (Creat3D, UK) and used in the second build. The second build (B02) used 100% recovered powder (no fresh powder added) from B01. The third build used 100% powder recovered from B02, hence labelled B03. This was repeated up to B10.

2.2. PA11 Powder usage Analysis

Since, in each build following B01, 100% of the used powder is used, the quantity of powder input reduced from B01 (6Kg) to B10 (0.5 Kg). The percentage of fused powder to total powder used in a specific build and the amount of powder wasted per unit powder recovered were measured to correlate the effect of the number of reuses to the amount of powder being recovered in each build. The weight of the built parts per unit fused powder in the build was also measured to confirm whether the number of reuses affects the density of the sample built.

Preprints (www.preprints.org) | NOT PEER-REVIEWED | Posted: 18 October 2023 doi:10.20944/preprints202310.1195.v1

2.3. Dimensional Accuracy Measurement

A FARO Edge Scan Arm HD (FARO Technologies UK Ltd, UK) with accuracy: ±35 μm and Scan Rate: 45,120 points/sec was used to 3D Scan the tensile test pieces . Each specimen was positioned in its print orientation when scanned, E.g. the XZ plane as shown in Figure 1. Two scans were used to capture the full geometry of the specimen; the main scan captured most of the surfaces, then the specimen was rotated 180° to scan the bottom surface. The 3D scan of the specimen was post-processed, using Polyworks Inspector Software (3DScanners, UK), to remove any erroneous data points and fill holes in the polygonal mesh. It was then aligned to the reference CAD file using a Best-fit Data to Reference alignment method.

A Data Colour Map was used to compare the measured 3D scan with the nominal CAD file and illustrate the deviation. Standard calliper gauges were created to measure the gauge width and thickness of each specimen and calculate the deviation between the nominal CAD file and measured 3D scan data.

2.4. Density Measurement

The density cubes were used to measure the density of the PBF-LS PA11 parts from B01 (100% Virgin) to B10.

For the density measurement, the weight of the individual density cubes was measured in air, W_A using a high-performance analytical balance (Balance XPR, Mettler Toledo, UK). Their weights were then measurement in isopropyl alcohol, W_B. Using Archimedes Principle, the density, ϱ of the cubes was calculated using Equation (1):

$$\varrho = \frac{W_A}{(W_A - W_B)} (\varrho_O - \varrho_L) + \varrho_L \quad (1)$$

where ϱ_O is the density of isopropyl alcohol (0.78977 g/ cm^3 at 19.5 °C) and ϱ_L = Density of air (0.0012 g/cm^3)(Balance XPR Datasheet, Mettler Toledo, UK).

For each build, 3 density values were obtained (n=3). The average of the 3 was calculated and presented as Average ± S.E.M (Standard error of mean). One-way ANOVA was performed to analyse the difference between density data at a 95% confidence interval.

2.5. Thermal Property

To quantify their thermal properties, differential scanning calorimetry (DSC) tests were done on the PA11 specimens (B01, B03, and BA10) using a DSC4000 (Perkin Elmer, UK). DSC specimens of weight 6 ± 1 mg were exposed to a temperature ramp of 25 °C to 250 °C at a rate of 10 °C/min. They were then cooled down from 250 to 25 °C at the same rate [19]. Under a nitrogen flow rate of 40mL/min, 3 sets of measurements were obtained. The melting enthalpy of the specimens was calculated by integrating the endothermic peak using the TA instruments TRIOS software and the crystallinity, X_c, was calculated using Equation (2):

$$X_c = (\Delta H_m / \Delta H^0_m) \times 100\ \% \quad (2)$$

where ΔH_m is the melting enthalpy calculated from the endothermic peak (J/g) and melting enthalpy for 100% crystalline PA11 matrix is denoted by ΔH^0_m (Theoretical ΔH^0_m = 226.4 J/g) [19]. The average of the 3 data per sample were calculated and presented as Average ± S.E.M (Standard error of mean). One-way ANOVA was performed to analyse the difference between density data at a 95% confidence interval (CI).

2.6. Tensile Testing

The tensile testing was done with respect to ASTM 638-14 [Standard Test method for Tensile properties of plastics], using a Shimadzu universal tester, AG-X (Shimadzu, UK). At a humidity of 39%, the test was performed up to failure using a load cell of 100 kN at a speed of 5mm/min and an Epsilon 3542 axial extensometer (±25mm). The force and displacement data collected was used to

Preprints (www.preprints.org) | NOT PEER-REVIEWED | Posted: 18 October 2023 doi:10.20944/preprints202310.1195.v1

calculate the engineering stress and strain, following which the average tensile modulus, ultimate tensile strength, yield strength and breaking strain was calculated for each build.

For each build, 5 values were obtained for each property measured (n=5). The average of the 5 was calculated and presented as Average ± S.E.M (Standard error of mean). One-way ANOVA was performed to analyse the difference between density data at a 95% confidence interval.

3. Results

3.1. Powder bed fusion laser sintering of PA11

The percentage of fused powder to total powder (Fused + unfused powder) used for from B01 to B10 had a polynomial increase as shown in Figure 2 (a). When considering 100% reuse of powder in PBF-LS, the percentage of fused powder (F) could be related to the number of times the powder has been used (N) using the following equation:

$$F = aN^2 + bN + c \quad (3)$$

where a, b and c are fitting constants unique to the type of powder used in the PBF-LS process. For the PBF-LS of PA11, the values of a, b and c are 0.164, 0.955 and 3.091 respectively.

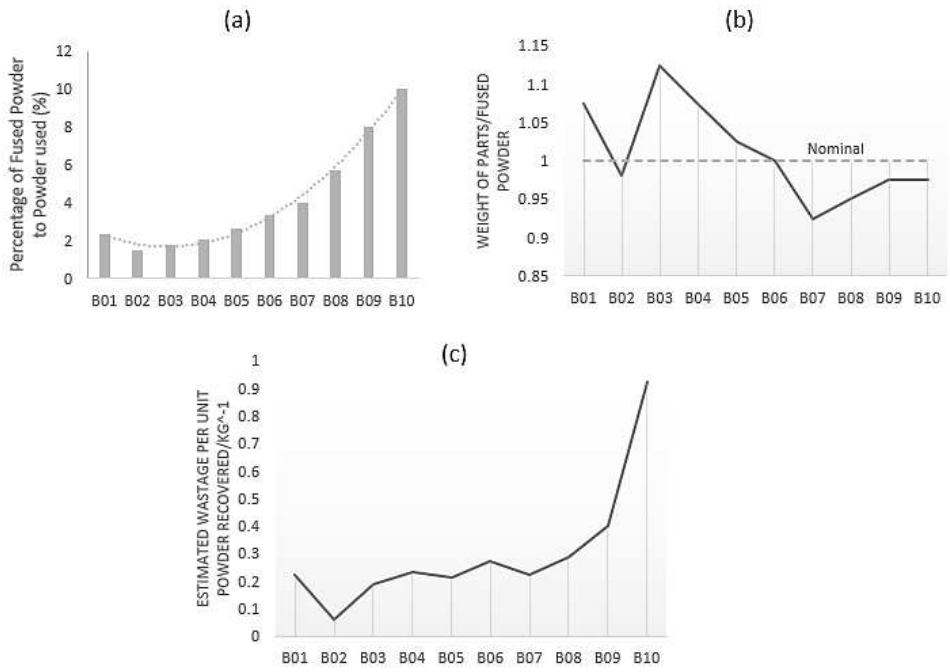

Figure 2. Usage of PA11 powder during the PBF-LS process from B00 to B09; (**a**) Percentage of fused powder to the amount of PA11 powder used; (**b**) Weight of the 3D printed parts as a ratio of the weight of PA11 powder fused and (**c**) Estimated waste of PA11 powder per unit mass of powder recovered.

The weight of all the parts printed from 1 build did not always match the weight of the fused powder. From B01 to B06, the weight of the samples was higher than that of the fused powder and lower from B07 to B10, as shown in Figure 2 (b). The higher weight was associated with polycondensation of the PA11 during the PBF-LS process which has been observed by Esposito et al. [17]. The increase in weight was associated with the post polymerisation condensation and associated humidity. The lower weight was associated with the shrinkage of PBF-LS polyamide parts [27]. For every unit of PA11 powder recovered for the next build, there was an increasing amount of waste from B01 to B10.

Preprints (www.preprints.org) | NOT PEER-REVIEWED | Posted: 18 October 2023 doi:10.20944/preprints202310.1195.v1

3.2. Dimensional Accuracy

Up to sample number 5 (B05; Figure 3(e)), the letters XZ and sample number could be read from the surface. On a macroscopic level, the increasing unevenness of the surface from B05 to B10 reduced the visibility of the letter and number engravings on the surface. The coarser surface observed with increasing number of reuse of PA11 powder was related to the higher viscosity and melting point of reused polyamide powders which remain unmolten on the surfaces of the 3D printed parts [5]. The high viscosity of the reused PA11 powder resisted the flow of the molten powder during the sintering process [25]. This coarse surface has been observed by other researchers as a result of using an PBF-LS process and has been associated with an 'orange-peel' effect [24].

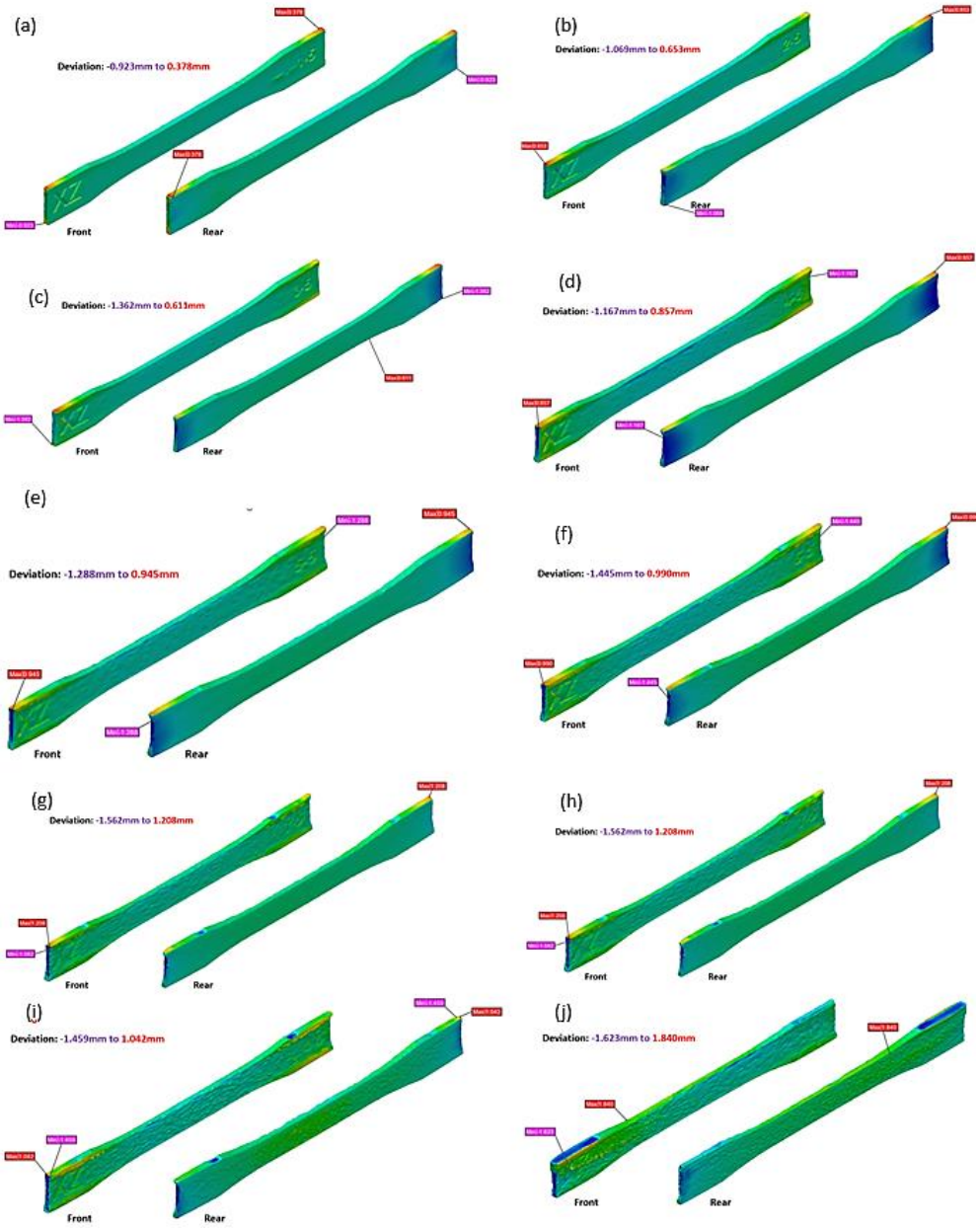

Figure 3. Colour Map showing deviation from CAD model for (**a**)-(**j**) B01 to B10 respectively.

The colour maps in Figure 3 represent the deviation of the PBF-LS PA11 samples from the nominal CAD file. The edges and corners experienced more deviation from the CAD as compared to flat surfaces with the deviation values comparison depicted in Figure 3. The gauge width represented the ZX build plane while the thickness represented the XY build plane. The thickness of samples was

Preprints (www.preprints.org) | NOT PEER-REVIEWED | Posted: 18 October 2023 doi:10.20944/preprints202310.1195.v1

mostly smaller than the CAD thickness as compared to the gauge width which was mostly larger than the CAD width as shown in Figure 4. This indicates shrinkage dominating the thickness as compared to condensation process and vice versa for the gauge width. It was also related to the ratio of the length to height which was 7.8:1 for the gauge section and 0.2:1 for the thickness section. Scan length is known to increase shrinkage along the X axis during a PBF-LS process resulting in shrinkage for the thickness [23].

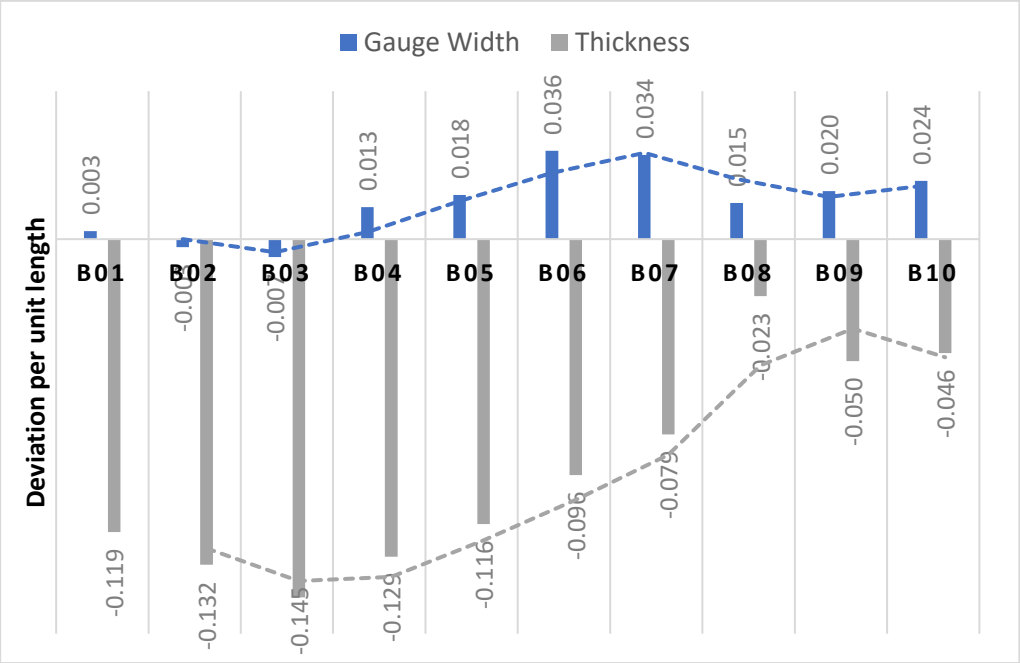

Figure 4. Deviation in gauge width and thickness of tensile test pieces during builds B01 – B10.

The deviation per unit length for the gauge width was minimal as compared to that for the thickness. The thickness deviation increased from B01 to B03 and then kept decreasing for the remaining builds. From B01 to B03, the PA11 powders are exposed to an elevated temperature for a short time resulting in few particles with high melting point. In those builds, there is still a homogeneous distribution of powder particles [28] which allowed the shrinkage effect to dominate due to the small scan length for the thickness section. From B03 to B10, there was an increasing number of PA11 particle with high melting point and low viscosity [5] which resulted in non-homogeneous distribution of the particles for the layer-by-layer process. This accounted for the uneven surface for the gauge section and this process dominated the effect of material shrinkage for thickness which resulted in a reduction in deviation from the nominal. This was confirmed by the decrease in density after B07 as shown in Figure 5. The increase in density from B01 to B03 was associated with the increase in molecular weight due to the polymerisation and cross-linking reactions during the PBF-LS process. The process increases the molecular chains resulting in an increase in molecular weight and hence density [16].

Preprints (www.preprints.org) | NOT PEER-REVIEWED | Posted: 18 October 2023 doi:10.20944/preprints202310.1195.v1

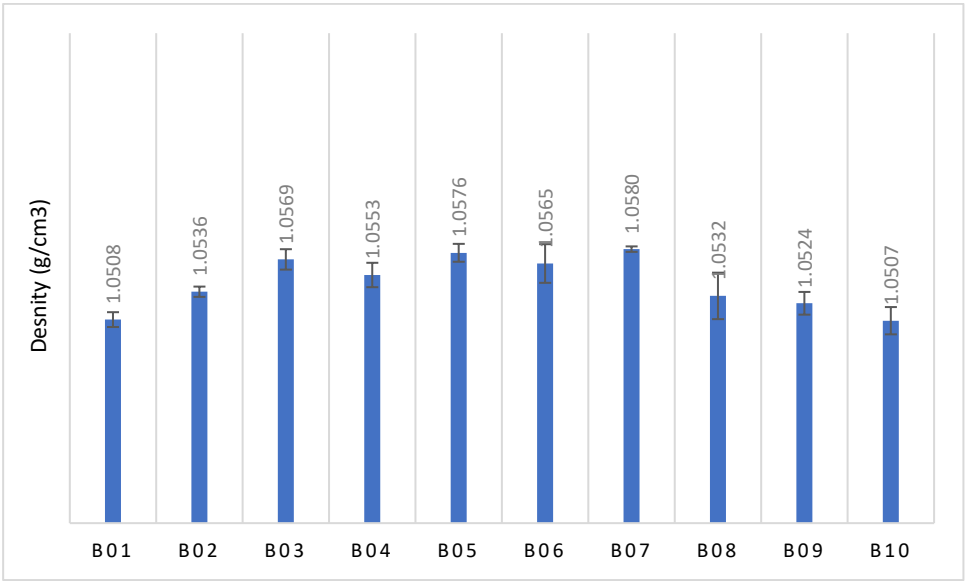

Figure 5. Density of the PA11 cubes from B01 to B10.

3.3. Thermal Properties

From the DSC thermograms obtained during the DSC analysis, as shown in Figure 6, the onset melting point (T_{OM}), peak melting point (T_{PM}), onset crystallisation point (T_{OC}), peak crystallisation point (T_{PC}) and melting enthalpy (ΔH) were obtained. The crystallinity was then calculated and presented in Table 2. For all the samples tested, the melt temperatures (onset and peak) were higher than that of the crystallisation temperatures (~25 °C). A delay in crystallisation prevents residual stress from building up resulting in less distortion due to the sintering process [9]. However, a higher temperature difference is associated with PA12 (~40 °C) [9] which could be associated with more distortion in PBF-LS PA11 parts as compared to PBF-LS PA12 parts.

The T_{OM}, T_{PM} and X (crystallinity) for the B01, B03 and B10 were significantly different from each other ($p = 0.000014$ (T_{OM}), 0.000005 (T_{PM}), and $p = 0.0003$ (X) at 95% CI). There was a decrease in X from virgin PA11 to 3rd use, following which there was an increase to 10th use (B10). Dadbakhsh et al. [5] made similar observation during the PBF-LS of PA12 reused powder, which was attributed to the crystal growth due to a post-condensation phenomenon. To further understand at which point, the crystallinity for PA11 samples started to increase after B03, DSC was performed on B04. As shown in Table 2, the crystallinity of B04 was significantly higher than B03 ($p = 0.01$) and slightly lower than B10 ($n=3$; CI=95%; $p=0.04$).

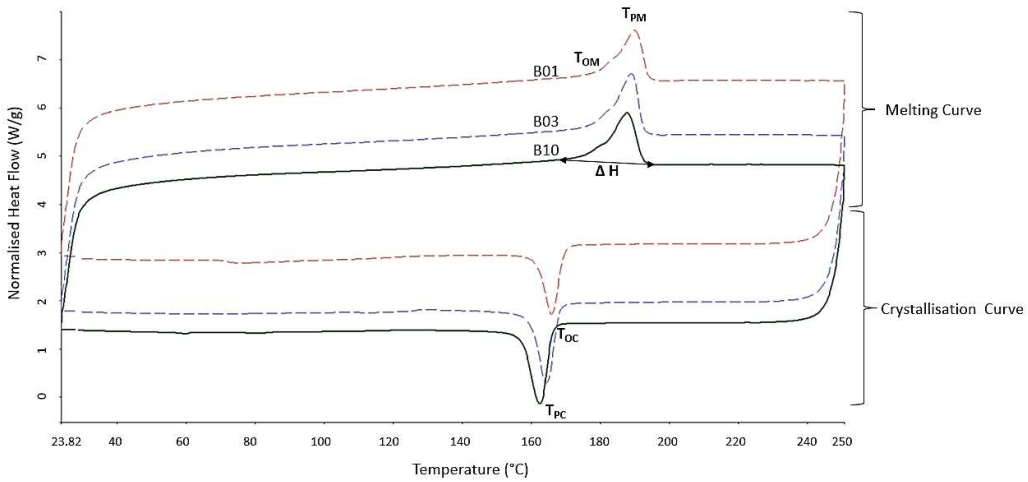

Figure 6. Sample DSC Thermograms of B01, B03 and B10.

Preprints (www.preprints.org) | NOT PEER-REVIEWED | Posted: 18 October 2023 doi:10.20944/preprints202310.1195.v1

Table 2. Thermal properties of B01, B03, B04 and B10.

Build	Onset Melting	Peak Melting	Enthalpy	Crystallisation Onset	Crystallisation Peak	Crystallinity
	T_{OM}	**T_{PM}**	**ΔH (J/g)**	**T_{OC}**	**T_{PC}**	**X_m (%) ± S.E.M**
B01	182.79	190.15	49.39	169.48	165.39	21.82 ± 0.04
B03	181.89	189.45	43.84	168.45	164.64	19.37 ± 0.13
B04	*182.21*	*189.19*	*49.45*	*168.17*	*165.8*	*21.84 ± 0.03*
B10	180.38	187.5	54.09	166.04	162.15	23.89 ± 0.46

The onset of crystallisation and peak crystallisation temperature decreased after the 4th use (B04) ($p=0.0005$) of PA11 powder for the process of PBF-LS. This agrees with what was observed for PA12 during repeated use [5] and was associated with the longer polymer chains post condensation. A decrease in T_{OC} and T_{PC} has been associated with ageing of such polyamides [2]. Hence, after the 4th use of PA11 in the Fuse1 Formlabs printer, the powder exhibited ageing characteristics.

3.4. Mechanical Properties

3.4.1. Ductility

Figure 7 (a) shows the typical stress – strain curve obtained from tensile test samples from B01 to B10. B01 to B05 exhibits a linear elastic behaviour with smooth hardening until failure. PA11 is a semi crystalline polymer consisting of orderly arranged polymer chains (Crystalline regions) and randomly arranged polymer chains (amorphous regions). When a tensile load is applied on a tensile test sample, the uniformly arranged polymer chains in the crystalline region resist deformation while the irregularly arranged chains slide easily. This is reflected by the stress-strain curve for B01, highlighting higher ductility. This was associated with necking observed in Figure 7 (d). When PA11 powder is reused, the polymerisation and cross-linking results in longer complex molecular change and hence more amorphous regions. This is expected to increase the intermolecular mobility resulting in higher ductility of B02 onwards. However, the opposite was observed, i.e. the ductility decreased when the powder is reused. Similar observation has been made for reused PA12 [5] which was related to the weaker bonding and coalescence in reused PA12 powder. From B05 to B10, an increasing brittle behaviour was observed which is due to an increase in the number of complex polymer chains and high viscosity and unmolten particles creating more defects in the build. Unmolten powder may also play a role in the nucleation and propagation of crack in the PA11 samples, leading to a decrease of ductility [16]. This brittleness identified in Figure 7 (a) is reinforced with Figure 7 (d) which shows the increased number of pieces in which the tensile samples fractured into.

Preprints (www.preprints.org) | NOT PEER-REVIEWED | Posted: 18 October 2023 doi:10.20944/preprints202310.1195.v1

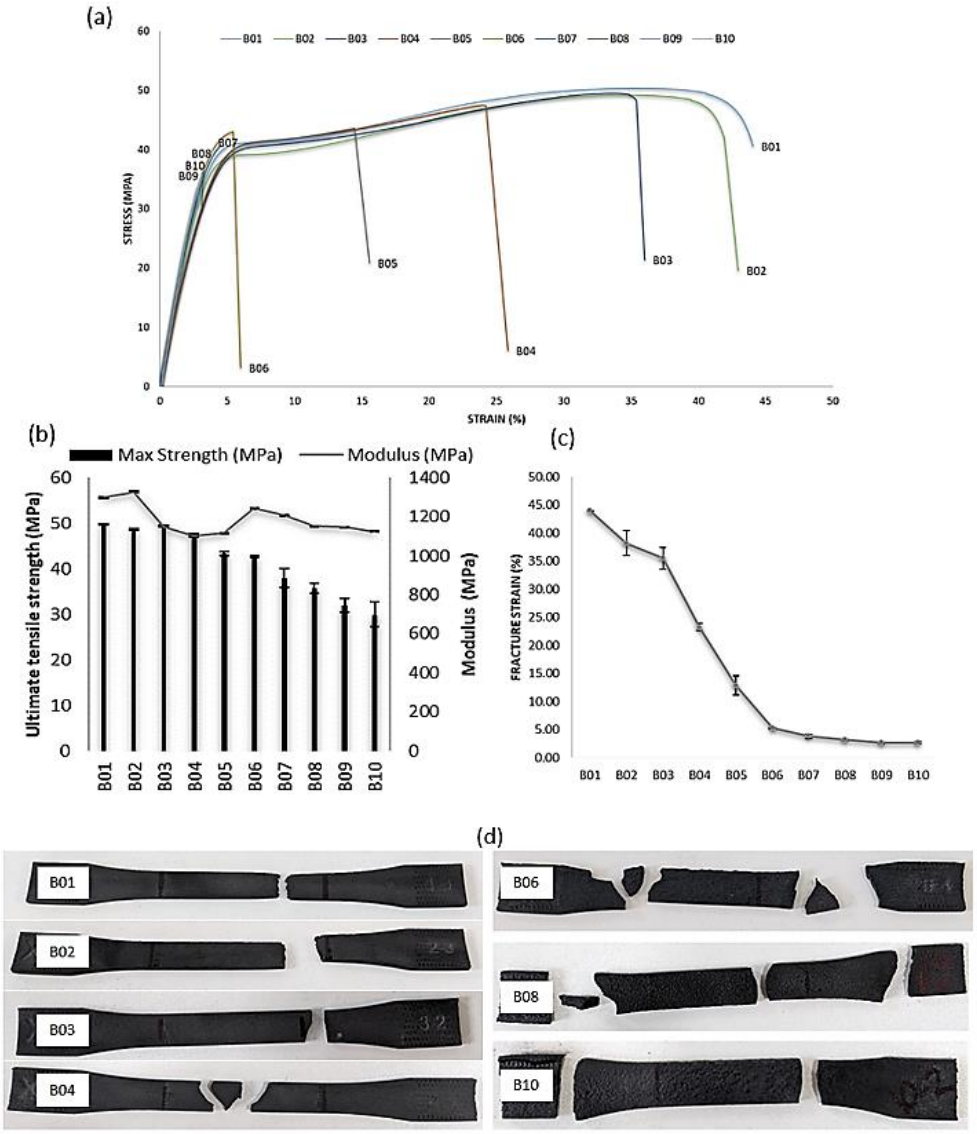

Figure 7. Tensile Test results for B01-B10. (**a**) Typical Stress Strain Curve from each build; (**b**) Average Ultimate Tensile Strength and Tensile Modulus and (**c**) Breaking Strain of samples from B01-B10 and (**d**) Typical fractured tensile samples for B01-B04, B06, B08 and B10.

3.4.2. Tensile Strength

The average Ultimate Tensile Strength, UTS of B01, B02 and B03 was 49.76 ±0.004, 48.61 ± 0.015 and 49.54 ± 0.008 MPa respectively as shown in Figure 7 (b). The UTS agrees with the values provided by the supplier as shown in Table 1. Although there was powder reuse from B01 (Virgin) to B03, there was no change in tensile strength from B01 to B03 (n=5; C.I.= 95%; p=0.2951). In the Fuse 1 Printer, the PA11 powder were exposed to a temperature of 193 °C which resulted in larger molecule formation post-polymerisation and cross linking. This has been associated with an enhancement of the intermolecular forces [16] which maintains the UTS from B01 to B03. Nonetheless, the UTS decreased significantly from B03 to B04 (n=5; C.I.= 95%; p=0.0006) to B10. Every use and reuse of the PA11 powder during the PBF-LS process, causes the powder to be exposed to a high temperature repeatedly. The powders which have been reused many times, in this case as from the 3rd reuse, have a higher melt viscosity [29] as compared to those powders in B01 to B03. Additionally, residual porosity is a common phenomenon during the PBF-LS of polymers [30]. Reusing PA11 powders, more than 2 times (No mixing with virgin powder), increases the porosity and hence the defects within the PBF-LS parts. This in turn reduces the tensile strength of the reused PA11 parts. Similar

 doi:10.20944/preprints202310.1195.v1

observations have been made for PA2200 [16], whereby reusing the PA2200 powder 2 times on its own, started to reduce the UTS. The decrease in UTS from B04 to B10 was also associated with an increase in crystallinity as shown in Table 2.

3.4.3. Tensile Modulus

There was no difference (n=5; C.I.= 95%; p=0.2529) between the tensile modulus of B02 (1327 ± 11.8 MPa) and B01 (Virgin PA11; 1298 ± 16.1 MPa). However, the modulus decreased significantly to 1149 ± 27.9 MPa for B03 (n=5; C.I.= 95%; p=0.003) and from B03 to B10, there was no significant change in modulus (n=5; C.I.= 95%; p=0.2302). In B01 and B02, there were stronger intermolecular forces which resisted movement during tensile loading. It is to be noted that the modulus of B01 is different from the ones provided by the manufacturer as shown in Table 1 (1.6 GPa). This was related to the build direction used for testing by the manufacturers which was in the XY direction while in this work, the ZY direction was used. The reduction in modulus from B03 was associated with the weakening intermolecular forces and increase in porosity and defects in the 3d printed parts due to the sintering process [16,30].

3.4.4. Yield Strength

The yield strength was calculated at 0.2% plastic strain. From B05 to B10, no yield strength (YS) data is available due to the brittle behaviour of the PBF-LS PA 11 parts. From B01 (YS = 19.49 ± 0.74 MPa) to B04 (YS = 17.47 ± 1.11 MPa) there was no significant difference in the yield strength (n=5; C.I.= 95%; p=0.2279). Up to the 4th use (B04), irrespective of the number of reuses, the stress that can be withstood by PA11 before plastic deformation is observed, is the same. The yield strength was related to the ductility of the respective samples.

3.4.5. Fracture Strain

The fracture strain of the virgin PA11 samples (B01) was significantly higher at 43.95%, as compared to any reused PA11 samples.(n=5; C.I.= 95%; p=0.0209). The fractured B01 samples depicted in figure 7 (d) confirms the high strain due to the necking before fracture, identified by the narrowing of the gauge width closer to the fracture site. The fracture strain for B02 and B03 was similar (n=5; C.I.= 95%; p=0.4624) after which there was a significant decrease in the fracture strain from B03 to B05 (n=5; C.I.= 95%; p=0.0021). During the reuse of the PA11 powders, the polymer chains become more complex with increasing molecular weight. This reduces the ability of polymer chains to undergo plastic deformation, hence reducing the fracture strain when reused. It was also observed that there was no change in the elongation at break from B05 to B10 (Figure 7 (c)). The reduction of ductility observed from B05 - B10 in Figure 7(a) was associated with the respective fracture strain and porosity due to PBF-LS [30] . In these sample, the tensile stress exceeds the applied stress resulting in defects/cracks formation in the samples at more than one location as shown in Figure 7(d). Thus, there is fracture before plastic deformation is observed. Similar observations have been made for PA2200 after the 4th reuse [16] .

4.0. Discussion

Polyamide 11 is a semi crystalline polymer with both regularly and irregularly arranged polymer chains. During the powder bed fusion laser sintering process, the powders are fused together using a laser source in the presence of nitrogen atmosphere. The unused powder is thus exposed to a high temperature, although the presence of nitrogen will prevent the thermo-oxidative degradation of the powder [31]. Nonetheless, when the unused powder undergoes the PBF-LS process again, the mechanical and thermal properties of resulting samples have been observed to change with accompanying changes in dimensional accuracy.

When using a virgin feedstock, the PBF-LS process generated PA11 samples with 21.8% crystallinity which is close to that of compression moulded PA11 (16%)[20]. Hence the Formlabs Fuse 1 printer can manufacture parts with similar crystallinity as traditionally manufactured PA11.

From B01 (100% Virgin Powder – 1st use) to B03 (100% 3rd use of powder), there was minimal deviation of gauge length from nominal and minimal change in tensile properties. This was associated with the increase in density of the PBF-LS parts (Figure 5) and hence an increase in the molecular weight. At large molecular weight, the polymer chains are long and more complex with stronger bonding with each other. Nonetheless, a decrease in crystallinity was observed from B01 to B03 (21.8% to 19.4%) which has been shown to decrease mechanical properties of polyamides such as PA12 [32]. PA12 is also a semi crystalline polymer with its sintered part having about 47% crystallinity when 100% virgin powder is used [15]. When reused, the latter decreased to 44 %. Chen et al. [15] also observed a more significant decrease in crystallinity from 47% to 23% for PA6. However, in comparison, the percentage of crystalline phase in PA11 is lower than PA12 and PA6. Hence the reduction in mechanical properties observed when PA12 is reused [32], is not reflected in PA11 in this work. When PA11 powder is used in a PBF-LS process and the remaining powder is reused for another 2 times, although there is a decrease in crystallinity following each use and reuse up to B03, the tensile strength and modulus did not degrade. This meant that the lower ratio of crystalline to amorphous regions in PBF-LS PA11 prevents the crystallinity to dominate intermolecular bonding in the latter and hence the mechanical properties.

From B04 to B10, an increase in crystallinity was observed to one higher than that of B01 [Virgin powder]. The repeated heating and cooling detangled the irregularly arranged polymer chains and arranged them more regularly in the 3rd (B03) and 4th (B04) use of the PA11 powder. Nonetheless the percentage crystallinity was still lower than that of PBF-LS PA12 observed by Chen et al. [15]. Similar to B01 – B03, the effect of crystallinity on tensile properties were not significant in B04 to B10. The significant decrease in tensile strength, modulus, fracture strain and ductility in the reused PBF-LS PA11 (B04 onwards) was thus associated with the increase in molecular weight and surface defects as identified in the results.

To further understand the exact mechanism behind the changes in physical and mechanical properties of PBF-LS PA11, the chemical ageing mechanism of PBF-LS PA11 needs to be further analysed; It will identify the specific change in polymer chains during reuse. Subsequently, the microstructural changes in PA 11 powder and the sintered PA11 during reuse in a PBF-LS process will reflect the chemical changes by visually distinguishing the polymer chains arrangement in the crystalline and amorphous phases. A study analysing the PA11 powder, its viscosity, rheology and powder surface topology will define the behaviour of the latter during a sintering process. The same analysis needs to be done on mixed PA11 powders (Virgin and reused) to understand the effect on refresh rates.

5. Conclusions

This paper investigated the effect of reusing PA11 powder during a powder bed fusion laser sintering process (PBF-LS), using a Formlabs Fuse 1 Printer, on the physical and tensile properties of the sintered PA11 parts. The following key observations were made:

a) Polyamide 11 is a semi crystalline polymer with about 22% crystallinity *which is lower than that of PA12*. Thus, the crystallinity of PA11 does not dominate the tensile properties of PBF-LS PA11.
b) When using the XZ build direction during a PBF-LS process, lower dimensions of sample thickness than CAD model were associated with shrinkage along the X- axis owing to the short scan length for thickness. Longer length sections such as gauge width had higher dimensions due to the condensation polymerisation of the PA11 polymer chains during sintering process.
c) The physical (density) and tensile (UTS, ductility, modulus and fracture strain) of PA11 is the same or better than virgin powder when reused up to 3 times (100% reuse, no mixing of virgin powder). As from 4th use, the tensile properties of the sintered PA11 sample degrades significantly with brittleness/ductility being the property being most affected.

This paper provides significant details on the impact of reusing PA11 powder in a PBF-LS process, without being mixed with virgin powder. It helps understand the fundamental of sintering semi-crystalline polymers with low crystallinity which can add value to ASTM F3456-22 for medical device additive manufacturing.

Author Contributions: Conceptualization, U.G. and P.W..; Methodology, U.G.; Validation, U.G.; Formal Analysis, U.G. Investigation, G.W. and M.P.; Resources, P.W. and U.G.; Data Curation, U.G.; Writing – Original Draft Preparation, U.G.; Writing – Review & Editing, M.P., Y.L. and P.W.; Visualization, U.G.; Supervision, P.W..; Project Administration, P.W.; Funding Acquisition, U.G. and P.W.

Funding: This research was partially funded by UKRI grant No. ES/X006573/1 and supported by ZINC.

Institutional Review Board Statement: In this section, you should add the Institutional Review.

Data Availability Statement: The data presented in this study are available upon request from the corresponding author.

Acknowledgments: The authors would like to acknowledge the support of the technical team in the Composites lab and Institute for Innovation in Sustainable Engineering at the University of Derby.

Conflicts of Interest: The authors declare no conflict of interest. The funders had no role in the design of the study; in the collection, analyses, or interpretation of data; in the writing of the manuscript; or in the decision to publish the results.

References

1. Peng, T., et al., *Sustainability of additive manufacturing: An overview on its energy demand and environmental impact.* Additive Manufacturing, 2018. **21**: p. 694-704.
2. Yang, F., et al., *A review of aging, degradation, and reusability of PA12 powders in selective laser sintering additive manufacturing.* Materials Today Communications, 2023. **34**: p. 105279.
3. Gornet, T., et al., *Characterization of selective laser sintering materials to determine process stability.* Solid Freeform Fabrication Symposium, 2002: p. 546-553.
4. Chen, P., et al., *Systematical mechanism of Polyamide-12 aging and its micro-structural evolution during laser sintering.* Polymer Testing, 2018. **67**: p. 370-379.
5. Dadbakhsh, S., et al., *Effect of PA12 powder reuse on coalescence behaviour and microstructure of SLS parts.* European Polymer Journal, 2017. **92**: p. 250-262.
6. He, D., et al., *Life cycle energy and greenhouse gas emissions implications of polyamide 12 recycling from selective laser sintering for an injection-molded automotive component.* Journal of Industrial Ecology, 2022. **26**(4): p. 1378-1388.
7. Kandis, M. and T.L. Bergman, *A Simulation-Based Correlation of the Density and Thermal Conductivity of Objects Produced by Laser Sintering of Polymer Powders.* Journal of Manufacturing Science and Engineering, 1999. **122**(3): p. 439-444.
8. Goodridge, R.D., C.J. Tuck, and R.J.M. Hague, *Laser sintering of polyamides and other polymers.* Progress in Materials Science, 2012. **57**(2): p. 229-267.
9. Drummer, D., D. Rietzel, and F. Kühnlein, *Development of a characterization approach for the sintering behavior of new thermoplastics for selective laser sintering.* Physics Procedia, 2010. **5**: p. 533-542.
10. Arkema, *Polyamide 11: the high-performance material of choice for production parts in Laser Sintering*, in *TCT Magazine*. 2016, Rapid News Publication Ltd.: Online.
11. Salazar, A., et al., *Monotonic loading and fatigue response of a bio-based polyamide PA11 and a petrol-based polyamide PA12 manufactured by selective laser sintering.* European Polymer Journal, 2014. **59**: p. 36-45.
12. Thokala, N., et al., *Characterisation of polyamide 11/copper antimicrobial composites for medical device applications.* Materials Science and Engineering: C, 2017. **78**: p. 1179-1186.
13. Tiwari, S.K., et al., *Selection of selective laser sintering materials for different applications.* Rapid Prototyping Journal, 2015. **21**(6): p. 630-648.
14. Wudy, K. and D. Drummer, *Aging effects of polyamide 12 in selective laser sintering: Molecular weight distribution and thermal properties.* Additive Manufacturing, 2019. **25**: p. 1-9.
15. Chen, P., et al., *Investigation into the processability, recyclability and crystalline structure of selective laser sintered Polyamide 6 in comparison with Polyamide 12.* Polymer Testing, 2018. **69**: p. 366-374.
16. Yao, B., Z. Li, and F. Zhu, *Effect of powder recycling on anisotropic tensile properties of selective laser sintered PA2200 polyamide.* European Polymer Journal, 2020. **141**: p. 110093.
17. Esposito, G.R., T.J. Dingemans, and R.A. Pearson, *Changes in polyamide 11 microstructure and chemistry during selective laser sintering.* Additive Manufacturing, 2021. **48**: p. 102445.
18. Ricou, P., E. Pinel, and N. Juhasz, *Temperature experiments for improved accuracy in the calculation of polyamide-11 crystallinity by X-ray diffraction.* Advances in X-ray Analysis, 2005. **48**.

19. Tey, W., C. Cai, and K. Zhou, *A Comprehensive Investigation on 3D Printing of Polyamide 11 and Thermoplastic Polyurethane via Multi Jet Fusion.* Polymers, 2021. **13**: p. 2139.
20. Di Lorenzo, M.L., A. Longo, and R. Androsch, *Polyamide 11/Poly(butylene succinate) Bio-Based Polymer Blends. LID - 10.3390/ma12172833 [doi] LID - 2833.* (1996-1944 (Print)).
21. Evans, R.S., et al., *Rapid manufacturing of silicon carbide composites.* Rapid Prototyping Journal, 2005. **11**(1): p. 37-40.
22. May, V., *Selective Laser Sintering: Advantages and Disadvantages*, in *Selective Laser Sintering*, P. UK, Editor. 2022, Prototal UK: Online: https://prototaluk.com/blog/selective-laser-sintering-advantages-and-disadvantages/.
23. Raghunath, N. and P. Pandey, *Improving accuracy through shrinkage modelling by using Taguchi method in selective laser sintering.* International Journal of Machine Tools and Manufacture, 2007. **47**: p. 985-995.
24. Dotchev, K. and W. Yusoff, *Recycling of polyamide 12 based powders in the laser sintering process.* Rapid Prototyping Journal, 2009. **15**(3): p. 192-203.
25. Yusoff, W., et al., *Influence of Molecular Weight Average, Degree of Crystallinity, and Viscosity of Different Polyamide PA12 Powder Grades on the Microstructures of Laser Sintered Part.* MATEC Web of Conferences, 2015. **26**: p. 03005.
26. Formlabs, *Materials Library: Functional Materials that look the part*, in *Quarterly*. 2023, Formlabs: Online: https://formlabs-media.formlabs.com/datasheets/1901266-TDS-ENUS-0.pdf.
27. Verbelen, L., et al., *Characterization of polyamide powders for determination of laser sintering processability.* European Polymer Journal, 2016. **75**: p. 163-174.
28. Singh, S., V. Sharma, and S. Anish, *Optimization and Analysis of Shrinkage in Selective Laser Sintered Polyamide Parts.* Materials and Manufacturing Processes, 2012. **27**: p. 707-714.
29. Craft, G., et al., *Impact of extended sintering times on mechanical properties in PA-12 parts produced by powderbed fusion processes.* Additive Manufacturing, 2018. **22**: p. 800-806.
30. Bourell, D., et al., *Performance Limitations in Polymer Laser Sintering.* Physics Procedia, 2014. **56**: p. 147–156.
31. Formlabs. *Formlabs SLS Product Security*. Getting Started with Fuse Sift 2023 [cited 2023; Available from: https://support.formlabs.com/s/article/Safety-with-Formlabs-SLS-products?language=zh_CN.
32. Chatterjee, S., F.A. Nüesch, and B.T.T. Chu, *Crystalline and tensile properties of carbon nanotube and graphene reinforced polyamide 12 fibers.* Chemical Physics Letters, 2013. **557**: p. 92-96.